Thermodiffusion of ions in nanoconfined aqueous electrolytes

Yuankai Yang [1,†,‡], *Xudong Zhang* [3,‡], *Zhiguo Tian* [1], *Guido Deissmann* [2], *Dirk Bosbach* [2], *Peng Liang* [3,*], *Moran Wang* [1,*]

[1] Department of Engineering Mechanics, Tsinghua University, 100084 Beijing, China.

[2] Institute of Energy and Climate Research (IEK-6): Nuclear Waste Management and Reactor Safety, Forschungszentrum Jülich GmbH, 52428 Jülich, Germany.

[3] School of Environment, Tsinghua University, 100084 Beijing, China.

ABSTRACT

Understanding of thermal effects on ion transport in porous media is very important for environmental applications. The movement of ions along a temperature gradient is named thermophoresis or thermodiffusion. In nanoporous media, where the interaction of ions with solid-liquid interfaces has a significant influence on their migration, the theoretical understanding of thermodiffusion is still incomplete. Herein, we present experimental results for the thermodiffusion of cations in saturated nanoporous silica by the through-diffusion method. Both the experimental data and theoretical analysis indicate that the temperature-induced polarization of surface charges strongly influences ionic transport. Stated simply, the electric field in a liquid electrolyte confined in nanopores changes when the applied temperature gradients are altered, thereby affecting the motion of the nanoconfined ionic species. By applying an external temperature field, the gradient of the surface charge density leads to the charged aqueous species exhibiting strong temperature gradient-dependent electrophoretic mobility. When the thickness of the electrical double layer is comparable to the size of the nanopores, the theory used herein indicates that this kind of nonisothermal ionic mobility is up to one order of magnitude larger than classical thermophoretic mobility. This study improves the understanding of the underlying mechanisms that govern the transport of ions in nanoporous media, which could set the stage for diffusional metamaterials induced by specific thermal fields.

KEYWORDS： thermodiffusion, nanoporous media, electrical double layer, electrophoretic.

SYNOPSIS： thermodiffusion in nanoporous media is an important fundamental process in many environmental and technical applications from desalination to nuclear waste storage.

GA

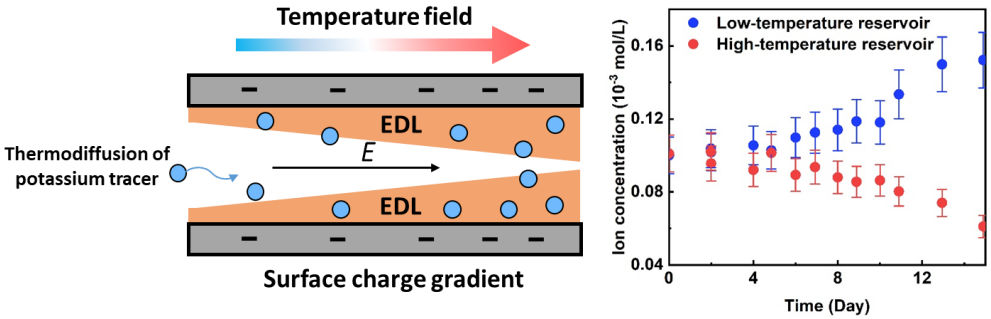
Temperature field
EDL
E
Thermodiffusion of
potassium tracer
EDL
Surface charge gradient
Low-temperature reservoir
High-temperature reservoir
Ion concentration (10^{-3} mol/L)
0.16
0.12
0.08
0.04
0
4
8
12
Time (Day)

1. INTRODUCTION

The Soret effect describes the motion of particles along a temperature gradient ∇T, also called thermophoresis or thermodiffusion. Thermodiffusion and its relevant effects have been investigated for a long time due to its relation to important applications, for example, the migration of radionuclides and other contaminants, cell physiology and energy conversion [1-4]. For a simple diluted electrolyte, the linear relationship between the thermodiffusive flux $\boldsymbol{J}_T$ and the temperature gradient ∇T is assumed to be $D_T C = \boldsymbol{J}_T / \nabla T$, with the proportion coefficient D_T as the thermodiffusion coefficient and an ion concentration *C*. By comparing to the ionic diffusivity in free water D_0, the Soret coefficient S_T is defined as the ratio $S_T = D_T / D_0$, which characterizes the magnitude of thermodiffusion; it is positive when an ion moves to the cold side of a system and negative when the ion moves to the hot side of a system. While a variety of investigations have promoted microscopic explanations of the Soret effect in a bulk system during the past few years [1, 5, 6], relatively few studies extend to confined systems such as nanoporous media.

Comparing to the bulk ones, the properties of the solid-liquid interface have more significant impacts on the physical and chemical characteristics of local electrolytes in a nanoconfined space, which further influences the transport of ionic species [7, 8]. Therefore, if the physicochemical properties of the solid-liquid interface are sensitive to temperature [9-11], species transport in nanopores might also be strongly responsive to an external temperature gradient. The electrical double layer (EDL) is a structure on

a charged surface, which is caused by the electrostatic interaction of ions with a surface and the thermal motion of ions. Its effect (the so-called electrokinetic effect) is one of the most important interfacial properties [12]. Previous studies indicated that the structure of the EDL is highly depended on the surrounding temperature [13, 14]. For instance, the surface reactivity of a solid, the permittivity of a confined electrolyte and the self-diffusion of ions related to the EDL are all strongly sensitive to the local temperature. Furthermore, a completely or partially overlapping EDL within nanopores might magnify the influence of temperature on the transport of nanoconfined ions [15, 16]. Several studies have already addressed isothermal ionic transport in nanoporous media at various temperatures [17, 18], yet the microscopic understanding of nonisothermal ionic transport in nanoporous media has remained unclear, especially from an experimental perspective.

In this work, we use the transport of potassium ions in a nanoscale membrane as an experimental system to address the above question. The diffusion of potassium tracers is implemented in nanoporous silica membranes (NPSMs) saturated with a NaCl electrolyte and various moderate temperature gradients are used along the transport direction. The experimental data show an abnormal inversion of the Soret coefficient of the confined potassium tracers, which is consistent with our proposed electrochemical model. We analytically and computationally show ion fluxes as a function of various thermal conditions and EDL thicknesses to address the significant role of an overlapping EDL on ion transport at the nanoscale with different thermal

gradients. These findings can also provide a critical and robust mechanism to manipulate contaminant transport and separation. In summary, this study unveils the remarkable roles of temperature as a controller that regulates the electrochemical properties of an interface and the transport of nanoconfined ions.

2. MATERIALS AND METHODS

2.1. Preparation of the nanoporous silica membrane (NPSM)

The NPSM is fabricated with sintered SiO_2 nanoparticles. Nanosized SiO_2 powder (particle size: 15±5 nm, purity: ≥99.8%, SSA: 250±30 m^2/g) was purchased from Zhongkehang, China. To decrease the viscosity of the concentrated nanoparticles, the nanosized SiO_2 powder was mixed with ultrapure water at a mass ratio of 1:9. The thick paste was then heated in an oven at 373 K for 24 hours to remove moisture. Polyvinyl alcohol (PVA, purity: ≥99.0%, source: aladdin)) was completely dissolved in ultrapure water to get 3%wt polyvinyl alcohol solution. Afterward, 1.38 g of the treated SiO_2 powder was fully blended with 0.2 mL of the dissolved polyvinyl alcohol solution, ground and sifted through a 100-mesh stainless steel sieve, then pressed in a cylindrical mold for 2 minutes (2~4 MPa). The nanosized SiO_2 sheet had a diameter of 3.1 cm and a thickness of 3.2 mm. It was later heated in a furnace at 1073 K in an air atmosphere to form a compact solid (NPSM). Morphological characterization of the NPSM was carried out by using scanning electron microscopy (GeminiSEM 500, Zeiss, China). The pore size distribution and specific surface area were measured using mercury

intrusion porosimetry (Autopore IV 9510, Micromeritics, USA) and a nitrogen adsorption analyzer (Tristar II 3020, Micromeritics, USA). Figure 1-A shows a typical scanning electron microscopy image of this porous silica at the nanoscale, which has a mean pore size $\bar{d}$ of 10~20 nm (Fig. S1-C).

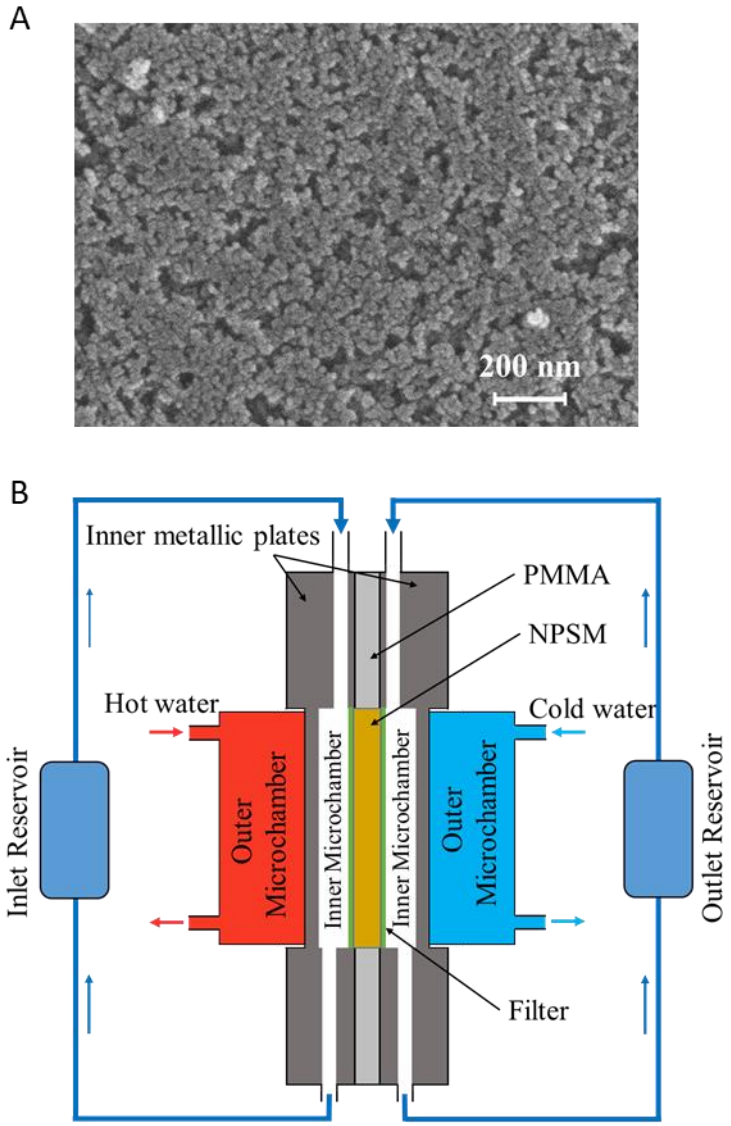

Figure 1 Schematics of the NPSM and the through-diffusion cell. (A) Typical SEM image of the tested NPSM and (B) schematic cross-section of the through-diffusion cell, which combines the NPSM (two photographs of the NPSM with millimeter- and micrometer-level resolutions are shown in Fig. S1) with two double-decker sheet-like microchambers.

2.2. Fabrication of the through-diffusion cell

The through-diffusion cell is a sandwich structure, and the NPSM is located at the middle layer, each side of which tightly bonds double-decker sheet-like microchambers. Figure 1-B illustrates the cross-section of this sandwich structure. The two outer metallic microchambers are stuck in the inner metallic plates. The cooled/heated ultrapure water at constant temperature, produced by a refrigerating machine and hot water bath kettle, quickly flows inside the outer microchambers to maintain their temperatures and create a steady thermal gradient inside the NPSM. Temperature sensors are attached to the outer metallic chambers to continuously monitor the real-time temperature variation. Two inner microchambers are the column-shaped flow channels carved inside the inner metallic plates and separated by the NPSM. The NPSM is embedded in a hollow polymethyl methacrylate (PMMA) plate and fixed by thermally insulated glue. Silicone pads are placed between the plates to avoid water leakage. The inner microchambers are partially open, and therefore, the electrolyte inside the inner microchambers can enter the NPSM. In addition, the inner microchambers are also connected with the outer reservoirs to create an electrolyte loop between the inner microchambers and outer reservoirs by a peristaltic pump. In this way, a mixed solution of sodium chloride (NaCl) and potassium iodide (KI) is pumped into each inner chamber and circulated (a detailed schematic is shown in Fig. S1-D). Herein, the background aqueous solution NaCl is used to maintain a steady ionic strength. Furthermore, the tracer concentration has to be significantly lower than the

NaCl concentration to avoid an interference on the local ionic strength. Potassium is chosen as tracer because its surface selectivity coefficient or binding energy sequence on silica surfaces is close to the of one of sodium [19, 20]. The flux of the potassium tracers through the NPSM is monitored by analyzing their concentration over time in the outer reservoirs on both sides; this method has been described in previous publications [21, 22].

3. RESULTS AND DISCUSSION

3.1. Diffusion of ions under isothermal conditions

The inner microchambers are first connected to the two outer reservoirs with a 1.0 mM NaCl solution to presaturate the NPSM. After a presaturation period of one week, the reservoirs are replaced. A new reservoir (inlet reservoir) containing 500 mL of 1.0 mM NaCl with a given tracer concentration (0.1 mM KI) is then connected to the inner microchamber on one side of the NPSM. The inner microchamber on the other side is connected to a new reservoir (outlet reservoir) containing 80 mL of 1.0 mM NaCl. Initially, the diffusion experiment is carried out at room temperature (298 K) to elaborate on the isothermal diffusion of ions in nanoporous media. Due to the difference in the tracer concentration between the two sides of the NPSM, the KI tracer diffuses into the low concentration reservoir; therefore, the concentration of the KI tracer increases over time. The low concentration reservoir is monitored at one-day intervals, and the ion concentration is analyzed by ion chromatography (ICS1000/2000, Dionex,

USA). In Figure 2-A, the points show the evolution of the tracer concentration over time in the low-concentration reservoir, where the potassium concentration increases much more drastically to reach a steady state compared with that of iodide. This is much different from KI transport in micrometer pores, where the electroneutrality is maintained in pore solution, thereby resulting in the same trend for both potassium and iodide ions [23]. Note that the silica surface is negatively charged when immersed in the given pore solution [24]. Therefore, the strong electrostatic interaction of the negatively charged surface with the nanoconfined ions can promote the diffusion of cations but inhibit that of anions within the nanopores of the NPSM, where electroneutrality is not present [25].

3.2. Diffusion of ions under nonisothermal conditions

After elaboration of the classical pattern for the isothermal diffusion of ions in nanoscale porous media, through-diffusion experiments under nonisothermal conditions were performed by using temperature gradients of 10, 20 and 30 K across the diffusion cell. After the same presaturation as in the isothermal experiments, the inner microchambers on both sides were connected to a new reservoir containing a NaCl solution (1 mM or 10 mM) mixed with 0.1 mM KI tracer. Here, we implement different temperature gradients on the NPSM by controlling the temperature at T_{in} = 313 K, 318 K and 323 K in the outer microchamber, while the temperature at the outlet is adjusted to T_{out} = 303 K, 298 K and 293 K, respectively; thus, the average

temperature is maintained at $\bar{T} = 308$ K. Accounting for the temperature drop across the filters on both sides, the actual temperature difference across the NPSM is $\Delta T = 0.914\left(T_{\text{out}} - T_{\text{in}}\right) = 9.1\,\text{K}, 18.3\,\text{K}, 27.4\,\text{K}$, respectively. The ionic Soret coefficient in the bulk solution becomes larger with decreasing salt concentration or increasing average temperature [5, 26]. For the given average temperature (308 K) and potassium tracer concentration (0.1 mM), previous experimental and theoretical studies [26, 27] indicated that the Soret coefficient of ions in bulk systems is positive and on the order of ~10^{-3} K^{-1}, which implies that the ions are thermophobic and move toward the cold region. However, as exemplarily shown in Figure 2-B, with a temperature gradient of 18.3 K and nanoconfinement, the potassium tracers exhibit opposite behavior compared to the bulk solution and move toward the high-temperature side.

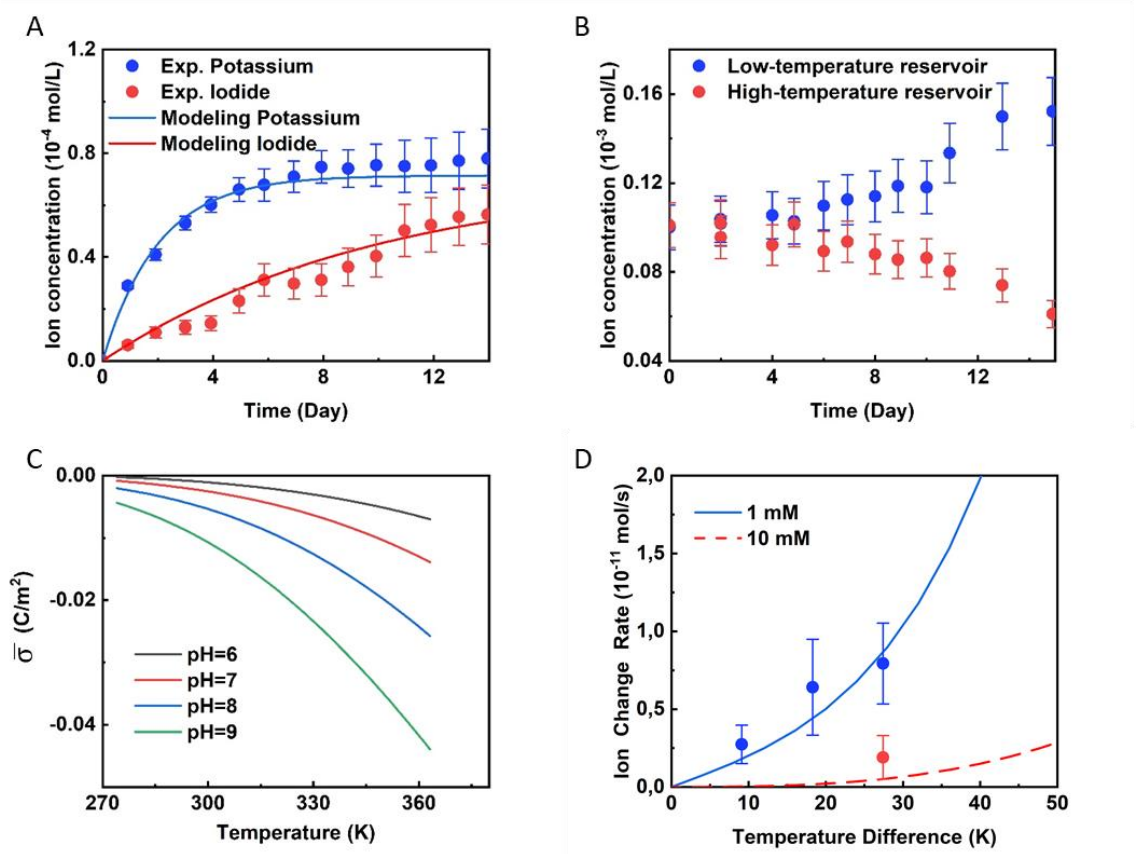

Figure 2 Experimental and modeling results in nanoconfined aqueous electrolytes. (A) Measured (squares) and modeled (lines) concentrations of potassium and iodide ions in the outlet reservoirs under isothermal conditions at room temperature. (B) Potassium concentrations in the reservoirs on both sides after applying a $\Delta T = 18.3$ K temperature difference. The background solution is 1 mM NaCl. (C) Effective surface charge density $\bar{\sigma}$ of the NPSM as a function of pH and temperature according to the temperature-dependent charge regulation model described in the Appendix ($C_0^r = 1$ mM). (D) Mean change rates δC of potassium ions in the outer reservoirs with different temperature differences ΔT in 1 mM and 10 mM NaCl electrolytes. The squares are the measured data, while the lines are calculated by our CTE (coupled thermal electrochemical) model.

3.3. Thermal-electrochemical coupling mechanism

To reveal the mechanisms of this unexpected thermodiffusion of nanoconfined potassium ions in the NPSM, we employ a coupled thermal electrochemical (CTE) model to analyze the different contributions to the ion flux. In the present system, with $\bar{u}_T$ being the thermoosmotically average velocity within nanopores in the NPSM, the

Péclet number is negligibly small $Pe = \bar{u}_T \bar{d} / D_0 \ll 1$ (see Appendix for details), indicating that compared with ionic diffusion, the ionic motion driven by thermoosmosis can be ignored. By simplifying a porous structure that includes pores and a solid matrix into a simple homogeneous medium, the effective diffusivity $D_{i,e}$ reflects the case in which the ith species demonstrates Fickian diffusion in this simple medium. The value of $D_{i,e}$ relates to the corresponding diffusivity in free water $D_{i,0}$ by a structure factor *G* as $D_{i,e}=D_{i,0} / G$ [28]. By treating the ions as point charges, the ion flux $\boldsymbol{J}_i$ can be described as [29-31]:

$$\boldsymbol{J}_i = -D_{i,e}\nabla C_i - D_{i,e} z_i C_i \nabla \psi^* - D_{i,e} S_T C_i \nabla T \,, \tag{1}$$

with an ionic valence z_i and a dimensionless electric potential $\psi^* = F\psi / RT$. In the above equation, F and R are the Faraday constant and ideal gas constant, respectively. The first two terms on the right-hand side of Eq. (1) account for Fickian diffusion and electrophoresis, given by the Nernst-Planck equation. The last term is used to calculate the thermodiffusive flux. Regarding a simple symmetric pore solution in charged porous media and using the Donnan theory together with the local charge balance of the pore solution with a solid surface, one finds the dimensionless local concentration of potassium ions [32, 33]:

$$C_i^* = C_i \,/ C_{i,b}^r = \mathrm{z}_i \rho / 2 + \sqrt{\left(\rho / 2\right)^2 + 1}\,, \tag{2}$$

with the dimensionless volume charge density $\rho = -Q / FC_0^r$. In the above equation, the superscript "r" refers to the corresponding term in the reservoir, $C_{i,b}^r$ and C_0^r are the concentrations of the tracer and the sum of cation concentrations, respectively, and

Q is the charge density per volume carried by the solid matrix of the NPSM, which is calculated by $Q = \bar{\sigma} S$ with the effective surface charge density $\bar{\sigma} = \alpha\sigma$ (α is a scale factor) and the surface area per volume of the NPSM $S = 0.18\ \mathrm{nm}^{-1}$. The intrinsic surface charge density σ is calculated by a temperature-dependent charge regulation model detailed in the Appendix. The largest bulk electrolyte concentration used in our study is 10 mM, so the steric effect is negligible and the ions can be assumed as point charges. Using the assumption of the Boltzmann distribution, ψ^* can be calculated through $\psi^* = -\ln C_i^* / z_i$. As mentioned before, an overlapping EDL can significantly promote electrokinetic effects [15, 16]. Therefore, the ratio $\kappa\bar{d}$ of the mean pore size $\bar{d}$ with the Debye length κ^{-1} is applied to judge the level of EDL overlap, where $\kappa = \sqrt{F^2 z_i^2 C_0^r / \varepsilon RT}$ with the permittivity ε of the pore solution [34]. When $\kappa\bar{d} \ll 1$, the EDL fully overlaps, while it is negligibly thin when $\kappa\bar{d} \gg 1$. To address the major effects, identical $D_{i,0}(T) \equiv \bar{D}_{i,0}$ and $S_T(T) \equiv \bar{S}_T$ are assumed here, where $\bar{D}_{i,0} = 1.28 D_{i,0}$ and $\bar{S}_T = 0.0008\ \mathrm{K}^{-1}$ at the average temperature $\bar{T} = 308\ \mathrm{K}$; notably, $D_{i,0}$ and S_T slightly vary with *T*. By inserting Eq. (2) in Eq. (1), the fluxes of ions in an NPSM with a thickness of *L* and a diameter d_R (detailed in the Appendix) are obtained by:

$$J_i = -\frac{\bar{D}_{i,0}}{GL}\left\{\Delta C_i + \bar{C}_i \ln\left[C_i^*(T_{\mathrm{out}}) / C_i^*(T_{\mathrm{in}})\right] + \bar{S}_T \bar{C}_i (T_{\mathrm{out}} - T_{\mathrm{in}})\right\}, \tag{3}$$

where

$$\Delta C_i = C_i^*(T_{\mathrm{out}}) C_{i,\mathrm{out}}^r - C_i^*(T_{\mathrm{in}}) C_{i,\mathrm{in}}^r, \tag{4}$$

$$\bar{C}_i = \left[C_i^*(T_{\mathrm{out}}) C_{i,\mathrm{out}}^r + C_i^*(T_{\mathrm{in}}) C_{i,\mathrm{in}}^r\right] / 2. \tag{5}$$

Furthermore, the concentrations of tracers in the reservoirs at the inlet and outlet are obtained by integrating J_i over time during periods t_s, $C_{i,\mathrm{in}}^r = C_{i,b}^r - \pi d_R^2/(4V_{in}) \cdot \int_0^{t_s} J_i dt$ and $C_{i,out}^r = C_{i,b}^r + \pi d_R^2/(4V_{out}) \cdot \int_0^{t_s} J_i dt$.

In the isothermal case, $L = 3.2$ mm, $d_R = 30$ mm, $\bar{d} = 11.1$ nm, $V_{in} = 500$ mL and $V_{out} = 80$ mL. $\bar{D}_{\mathrm{I},0} = D_{\mathrm{I},0} = 2.05 \cdot 10^{-9}$ m^2/s and $\bar{D}_{K,0} = D_{K,0} = 1.96 \cdot 10^{-9}$ m^2/s at room temperature. The charge regulation model gives $\sigma = -0.0032$ C/m^2 at $C_0^r = 1$ mM, pH=6 and T=298 K. There are two unknown parameters G and α in the CTE model. By fitting the isothermal concentration profiles of tracers over time, we can determine the parameters G=3.0 and $\alpha = 0.31$, which is in the classical range of these parameters [35-37]. Figure 2-A compares the measured and modeled concentrations of potassium and iodide ions in the outlet reservoirs under isothermal conditions, where the lines are calculated based on the CTE model after fitting. These comparisons indicate that the CTE model successfully captures the effect of the EDL on ionic transport in the NPSM, which promotes cation transport while weakening anion transport.

Figure 2-C shows the effective surface charge density $\bar{\sigma}$ of the NPSM as a function of temperature and pH, which is calculated by the charge regulation model described in the Appendix. Here, $\bar{\sigma}$ tends to be more negative with increasing temperature at the same pH. This means that the surface has a more negative charge, therefore adsorbing more cations at higher temperatures, which is also proved by previous experimental studies [10, 18]. Therefore, after applying a thermal gradient to the NPSM, its surface

will be inhomogeneously charged. To reduce the fluctuations from experimental data on the results, the mean change rate $\delta C_i = \int_0^{t_s} SJ_i dt / t_s$ in the reservoir within a time interval $t_s = 1$ day is used here. We analyzed the δC_{K} of potassium under different nonisothermal conditions by using both the CTE model and experimental data (see Figure 2-D). We used the average diffusivities at T=308 K in the CTE model: $\bar{D}_{\mathrm{I},0} = 1.28 \times 2.05 \cdot 10^{-9}$ m^2/s and $\bar{D}_{K,0} = 1.28 \times 1.96 \cdot 10^{-9}$ m^2/s. The results show good agreement between the modeling results and experimental data; as expected, a larger temperature difference ΔT induces a larger δC_{K}. By increasing the concentration of the background electrolyte NaCl from 1 mM to 10 mM, the EDL becomes thinner and δC_{K} obviously decreases, revealing the critical role of the EDL on the transport of potassium ions during nanoscale confinement.

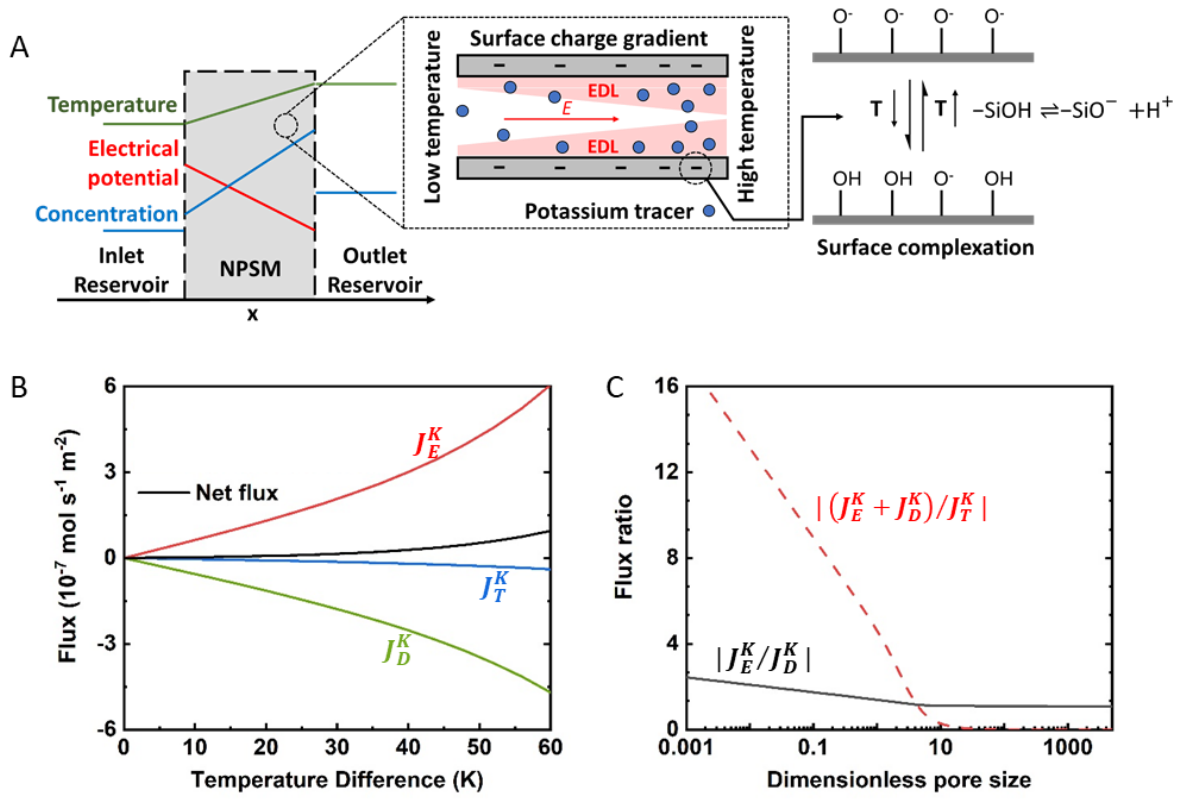

Figure 3 Mechanism and flux proportions after applying temperature gradients. (A) The figure on the right side shows the mean concentration, electrical potential and temperature profiles within the NPSM and a microscopic sketch of the potassium tracer and EDL in a single nanopore with an applied temperature gradient (middle); the red areas represent the EDL. The side with a high temperature has a larger EDL thickness, so it can adsorb more potassium ions. The red arrow denotes the inner electrical field *E*. The figure on the left side shows the patterns of surface complexations with respect to temperature. (B) Potassium flux due to pure diffusion $J_D^K = -D_{K,e}\nabla C_K$, electrophoresis $J_E^K = -D_{K,e}C_K\nabla\psi^*$, and thermophoresis $J_T^K = -D_{K,e}S_TC_K\nabla T$, and the net flux as a function of ΔT (the positive direction of flux is along the positive x-axis in (A). (C) Flux ratios $\left|J_E^K / J_D^K\right|$ and $\left|\left(J_E^K + J_D^K\right) / J_T^K\right|$ as a function of the dimensionless pore size $\kappa\bar{d}$ (at $\Delta T = 40$ K).

Considering Eq. (1), potassium transport is driven by three terms: pure diffusion $J_D^K = -D_{K,e}\nabla C_K$, electrophoresis $J_E^K = -D_{K,e}C_K\nabla\psi^*$ and thermophoresis $J_T^K = -D_{K,e}S_TC_K\nabla T$. Based on the CTE model, we analyzed the flux proportions from these three terms with different thermal gradients (Figure 3-B). The results indicate that the absolute values of flux from all three terms increase when applying a larger temperature gradient. The absolute value of J_E^K is slightly larger than that of J_D^K, while both of them are much larger than that of J_T^K. Moreover, J_E^K and J_D^K show larger changes than J_T^K when the temperature gradient is changed, while the directions of J_E^K and J_D^K show completely opposite tendencies. As presented in Figure 2-C, this is caused by the surface charge density gradient on the silica surface, which is induced by the applied temperature gradient. Here, the surface charge density, as well as the related mean electrical potential within the nanopores, reach more negative values on the high-temperature side. Hence, the electric field $-\nabla\psi$ has a direction opposite to the high-temperature side and causes the electrophoresis of cations in the same direction as the electric field. As illustrated by Figure 3-A, since the higher temperature side can adsorb more cations, the direction of J_D^K is opposite to J_E^K toward the low-

temperature side. To quantitatively compare the magnitudes of J_D^K, J_E^K and J_T^K, we analyzed two ratios $\left|J_E^K / J_D^K\right|$ and $\left|\left(J_E^K + J_D^K\right) / J_T^K\right|$ as a function of the dimensionless pore size $\kappa\bar{d}$ in Figure 3-C, where C_0^r is changed to achieve the variation of $\kappa\bar{d}$ at a constant $\Delta T = 40$ K. The results show that both $\left|J_E^K / J_D^K\right|$ and $\left|\left(J_E^K + J_D^K\right) / J_T^K\right|$ decrease with increasing $\kappa\bar{d}$. In addition, regarding $\kappa\bar{d}$ up to 10^3, $\left|J_E^K / J_D^K\right|$ is always larger than one (or $\left|J_E^K\right| > \left|J_D^K\right|$). This means that the sum of $J_E^K + J_D^K$ will be in the same direction as J_E^K despite the opposite directions of J_E^K and J_D^K. $\left|\left(J_E^K + J_D^K\right) / J_T^K\right|$ will approach zero as $\kappa\bar{d} \to \infty$, where the EDL thickness is negligibly small compared to the pore diameter. In this case, thermodiffusion is dominant for the net flux, and the EDL effect can be ignored. In contrast, $\left|\left(J_E^K + J_D^K\right) / J_T^K\right| \to \infty$ as $\kappa\bar{d} \to 0$ represents a fully overlapping EDL. This means that an overlapping EDL remarkably magnifies electrophoresis. Hence, $\left|J_E^K + J_D^K\right|$ governs the net flux, while thermodiffusion is negligible. For instance, if $\kappa\bar{d} < 10^{-2}$, one finds that $\left|J_E^K + J_D^K\right|$ will be larger by one order of magnitude compared to $\left|J_T^K\right|$. In our experiments, $\kappa\bar{d} \approx 1.2$ and $\left|\left(J_E^K + J_D^K\right) / J_T^K\right|$ are approximately 4 for the case of a 1 mM NaCl solution. Regarding the case of a 10 mM NaCl solution, $\kappa\bar{d} \approx 3.9$ while $\left|\left(J_E^K + J_D^K\right) / J_T^K\right|$ is approximately 1.3, which is slightly larger than 1. Therefore, in both cases, the thermodiffusion contribution to the potassium flux is smaller than from the electrophoresis contribution, which is consistent with our experimental results with a positive δC_{K}.

3.4. Fully numerical simulations of transport

The electrokinetic response concerned in this work may be different to those with a constant or temperature-dependent value of $D_{i,0}$. In particular, the overlapping EDLs in nanopores could magnify this difference further [38]. It is worth of mentioning that the validity of the Gouy−Chapman model or the Donnan model is questionable as the EDL overlaps in pores [33, 39, 40]. Such problems can be solved by using fully coupled Poisson-Nernst-Planck (PNP) simulations with the temperature-dependent properties [41]. By applying a temperature gradient through the membrane, the concentrations of tracers will be different in the inlet and outlet reservoirs. After reaching steady state, the concentration difference $\Delta C_s^r = C_{i,\mathrm{out}}^r - C_{i,\mathrm{in}}^r$ between the two reservoirs will be constant. Using the developed CTE model, the relative concentration difference $\Delta C_s^* = \Delta C_s^r / C_{i,\mathrm{in}}^r$ at steady state as a function of temperature difference ΔT can be derived as $J_i = 0$, which gives:

$$\Delta C_s^* = \frac{2C_{\mathrm{K}}^*(T_{\mathrm{in}}) + C_{\mathrm{K}}^*(T_{\mathrm{in}})\ln\left[C_{\mathrm{K}}^*(T_{\mathrm{in}})/C_{\mathrm{K}}^*(T_{\mathrm{out}})\right]}{2C_{\mathrm{K}}^*(T_{\mathrm{out}}) - C_{\mathrm{K}}^*(T_{\mathrm{out}})\ln\left[C_{\mathrm{K}}^*(T_{\mathrm{in}})/C_{\mathrm{K}}^*(T_{\mathrm{out}})\right]} - 1. \quad (6)$$

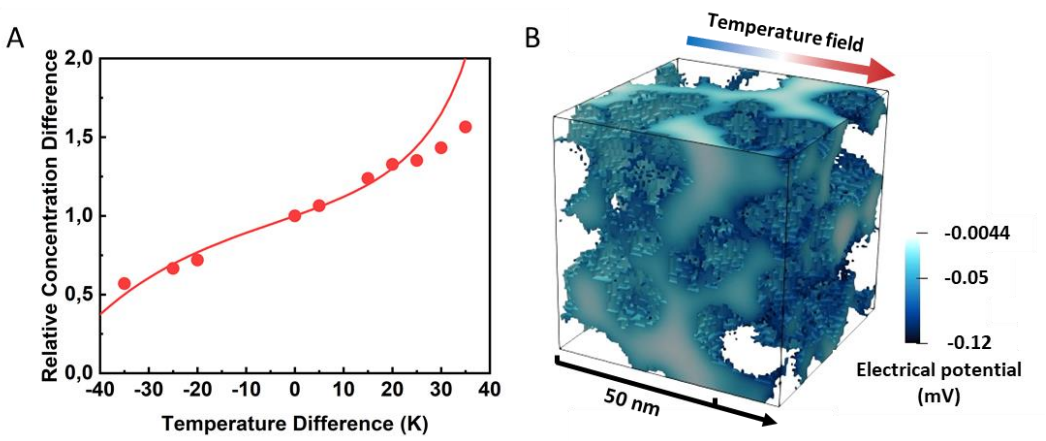

Figure 4 Modeling results of the nonisothermal diffusional at steady state. (A) Relative concentration difference $\Delta C_s^* = \Delta C_s^r / C_{i,\mathrm{in}}^r$ as a function of the temperature difference ΔT at steady state, calculated by our CTE model (solid line) and numerical framework (circle symbols). (B) Simulated three-dimensional distribution of the electrical potential under a temperature gradient ($\Delta T = 35$ K). Solid phase is invisible.

Figure 4-A shows that ΔC_s^* increases with an increasing ΔT. Herein, the results (solid line) by our model depend on the average diffusivities and the mean concentrations of ions in Eq. (6) at pH=8 and $C_0^r = 0.01$ M. We also simulated the same processes by numerically solving the fully coupled PNP equations. The main process of our numerical framework is described in the Appendix. The simulation results (circle symbols in Figure 4-A) agree well with the solution from the CTE model , as $|\Delta T| < 35$ K, which again supports the accuracy of the CTE model. Figure 4-B presents the simulated electrical potential distribution in a three-dimensional nanoporous membrane under applying a temperature field, where the pores with a higher temperature show a lower electrical potential.

Our experimental and modeling results reveal the critical impact of an overlapping EDL on thermodiffusion in nanoscale porous media. With a temperature gradient, the induced surface charge gradient at the solid-liquid interface will create an inhomogeneous EDL structure along the transport direction, which could significantly enhance ionic transport. Furthermore, our findings have the potential to become a fundamental method for manipulating macroscopic ion transport. Inspired by the thermal metamaterials developed several years ago [42-45], the mechanisms in this study could be implemented for diffusional metamaterials, where ionic diffusion is

governed by a temperature field. For instance, if a spot-like heater (the temperature field shown in Figure 5-B) is applied to a 2D ideal nanoscale structure (Figure 5-A), the cationic tracers could also accumulate in this region; thus, a spot-like heater acts similar to a thermal concentrator. Figure 5-C and Figure 5-D compare the PNP simulations for concentrating the cationic tracers by turning the heater on or off (also see more details in Movie S1 for comparison). The simulations show that the cationic tracer is obviously concentrated in the center of this nanoporous medium when it is heated, which can potentially be used to separate contaminants.

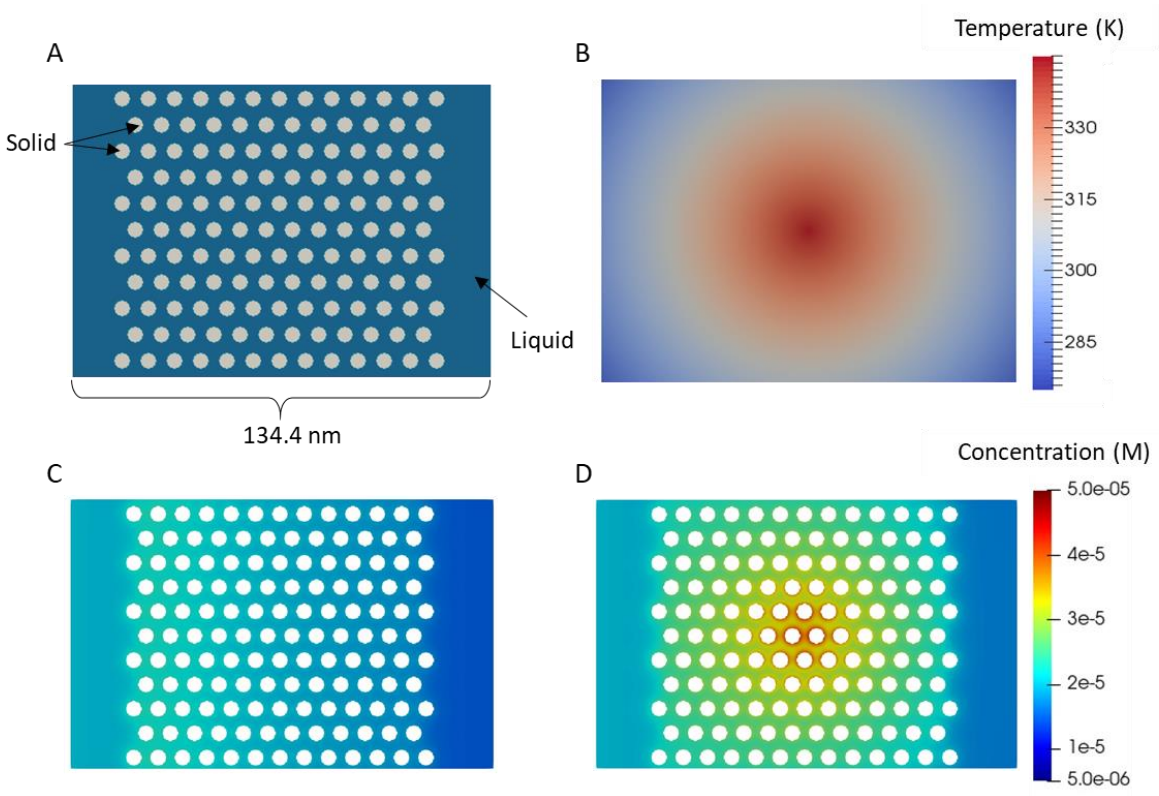

Figure 5 Manipulate ionic transport in nanoporous media by controlling the temperature field. (A) 2D nanoporous structure in our simulation. (B) Steady-state temperature field if the heater is on. (C) and (D) Simulated distribution of the cationic tracer concentration when turning the heater on and off (also see Movie S1 for comparison).

4. CONCLUSION

Thermodiffusion in nanoporous media is an important fundamental process in many natural and technical settings. We demonstrate that the gradient of the surface charge density induced by the applied temperature field leads to electrophoretic ionic mobility, which may promote up to one order of magnitude larger ionic mobility than classical thermophoretic mobility. Both experimental and modeling results in this study indicate the remarkable effect of temperature on the transport of nanoconfined ions. Furthermore, our results provide a critical and robust mechanism to manipulate ionic transport, which can be applied in energy conversion, species separation/collection, or desalination. This manipulation method does not need a subtly designed structure, only requiring the application of a suitable temperature field on nanoporous materials. In addition, the surfaces of most mineral materials (such as clay, silica or calcite) are naturally charged when in contact with an electrolyte, and the surface charge automatically changes with varying temperature, which is easier than other manipulation methods [16, 46, 47]. Therefore, compared with other manipulation methods, this mechanism is convenient, nondestructive and extensive.

ASSOCIATED CONTENT

Supporting Information.

The following files are available free of charge.

The calculation of Péclet number; details on the derivation of flux formulae and the pore-scale numerical framework; figures showing more details of the NPSM and the measurement setup; a movie showing the evolutions of cations and anions in 2D porous media.

AUTHOR INFORMATION

Corresponding Author

* mrwang@tsinghua.edu.cn (MW). * liangpeng@tsinghua.edu.cn (PL)

Present Addresses

† Now at Institute of Energy and Climate Research (IEK-6): Nuclear Waste Management and Reactor Safety, Forschungszentrum Jülich GmbH, 52428 Jülich, Germany.

Author Contributions

Y.Y., X.Z. and M.W. designed the research; Y.Y., X.Z., and Z.T. performed the research; Y.Y., X.Z. and M.W. analyzed the data; the manuscript was written through contributions of all authors. All authors have given approval to the final version of the manuscript.

‡ Y.Y. and X.Z. contributed equally.

Notes

The authors declare no competing financial interest.

ACKNOWLEDGMENT

This work is financially supported by the National Key R&D Program of China (No. 2019YFA0708704), the NSF grant of China (No. U1837602, 51676107) and the Tsinghua University Initiative Scientific Research Program. G.D. and D.B. acknowledge the funding received from the German Federal Ministry of Education and Research (BMBF, grant agreement 02NUK053A) and from the Initiative and Networking Fund of the Helmholtz Association (HGF grant SO-093) within the collaborative project iCross.

APPENDIX

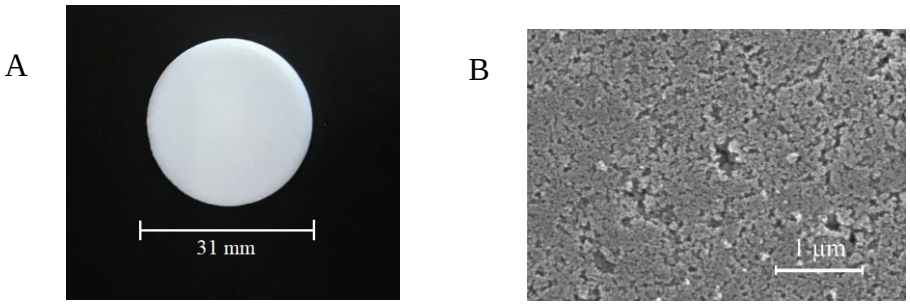

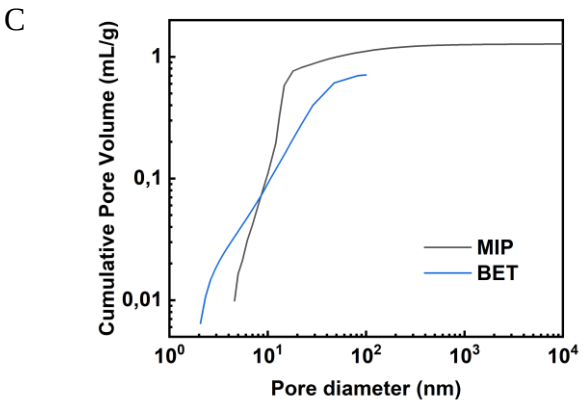

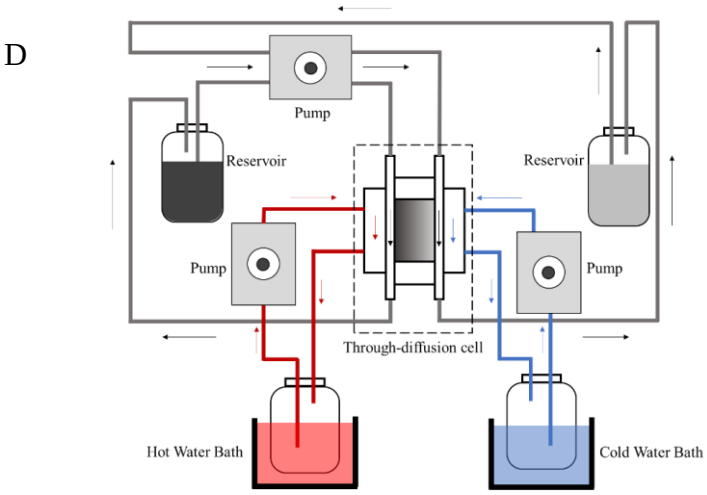

Fig. S1. (A) A photograph of the nanoporous silica membrane (NPSM); (B) a typical SEM image of the tested NPSM at the micrometer scale; (C) pore size distribution of the tested NPSM derived from mercury intrusion porosimetry and N_2 adsorption measurement; (D) schematic of the measurement setup.

Péclet number. As derived by Dietzal and Hardt [15], in a long straight nanochannel with the channel size $\bar{d}$, length L and surface zeta potential ζ, the thermoosmotically velocity of a aqueous electrolyte is given by:

$$u_T\big|_{\max} \approx u_{HS}\left\{\left[1-\frac{1}{\cosh(\bar{\kappa})}\right]\frac{\tanh(\bar{\kappa})}{\bar{\kappa}}+T\frac{d_T\varepsilon}{8\varepsilon}\left[\frac{\bar{\kappa}^2}{\cosh^2(\bar{\kappa})}-\tanh^2\left(\cosh(\bar{\kappa})\right)\right]\right\}, \quad \text{(S7)}$$

where $\bar{\kappa}=\bar{d}/\lambda_{\mathrm{DB}}$ and $u_{HS}=\varepsilon\zeta^2\eta^{-1}L^{-1}\Delta T/\bar{T}$ denote the dimensionless channel width and the thermally induced Helmholtz-Smoluchowski velocity. For a 1 mM NaCl electrolyte, the Debye length λ_{DB} is around 10 nm [34], permittivity $\varepsilon=6.95\times10^{-10}\ \mathrm{C/V\cdot m}$, $d_T\varepsilon/\varepsilon=-5.1\times10^{-3}\ \mathrm{K^{-1}}$ [48] and dynamic viscosity $\eta=10^{-3}\ \mathrm{Pa\cdot s}$. Here, the zeta potential of silica is set as about $-25\ \mathrm{mV}$. For the maximum temperature difference $\Delta T=30\ \mathrm{K}$ at a mean temperature $\bar{T}=333\ \mathrm{K}$ as used in the main text, and using the parameter values as given above, one can get:

$$Pe=\bar{u}_T\bar{d}/D_0<u_T\big|_{\max}\bar{d}/D_0<\bar{d}/L\,. \quad \text{(S8)}$$

Note that $\bar{d}/L\ll1$ for a long straight nanochannel. Hence Pe is much smaller than 1.

Derivation of the average flux formula. To model the transport in our experiment, we start from the Nernst-Planck equation defined by Eq.(1). For the investigated system depicted in Fig. S2, the gradients of ion concentration, electrical potential and temperature are calculated by the difference approximation: $\nabla C_i\approx\Delta C/L=\left(C_{i,\mathrm{out}}-C_{i,in}\right)/L$, $\nabla\psi^*\approx\left(\psi^*_{\mathrm{out}}-\psi^*_{\mathrm{in}}\right)/L$ and $\nabla T\approx\left(T_{\mathrm{out}}-T_{\mathrm{in}}\right)/L$ within the membrane. Together with eq. (2), one finds $\nabla C_i\approx\left[C_i^*\left(T_{\mathrm{out}}\right)C^r_{i,\mathrm{out}}-C_i^*\left(T_{\mathrm{in}}\right)C^r_{i,\mathrm{in}}\right]/L$. Further $\nabla\psi^*$ can be calculated by using Ξ_i as $\nabla\psi^*\approx\ln\left[C_i^*\left(T_{\mathrm{in}}\right)/C_i^*\left(T_{\mathrm{out}}\right)\right]/z_iL$. Herein, we employ the average concentration $\bar{C}_i=\left[C_i^*\left(T_{\mathrm{out}}\right)C^r_{i,\mathrm{out}}+C_i^*\left(T_{\mathrm{in}}\right)C^r_{i,\mathrm{in}}\right]/2$ to approximately estimate the electrophoretic and thermophoretic terms. Therefore, the eq. (3) can be rewritten into:

$$J_i = -D_{i,e}\left\{\frac{\left[C_i^*\left(T_{\text{out}}\right)C_{i,\text{out}}^r - C_i^*\left(T_{\text{in}}\right)C_{i,\text{in}}^r\right]}{L} + \frac{\bar{S}_T\left[C_i^*\left(T_{\text{out}}\right)C_{i,\text{out}}^r + C_i^*\left(T_{\text{in}}\right)C_{i,\text{in}}^r\right]\left(T_{\text{out}} - T_{\text{in}}\right)}{2L}\right.$$

$$\left. + \frac{\left[C_i^*\left(T_{\text{out}}\right)C_{i,\text{out}}^r + C_i^*\left(T_{\text{in}}\right)C_{i,\text{in}}^r\right]\cdot\ln\left[C_i^*\left(T_{\text{in}}\right)/C_i^*\left(T_{\text{out}}\right)\right]}{2L}\right\}. \quad \text{(S9)}$$

By using the structure factor $G=\bar{D}_{i,0}/D_{i,e}$ to account for the tortuosity and connectivity, eq (S9) can be finally simplified to eq (3).

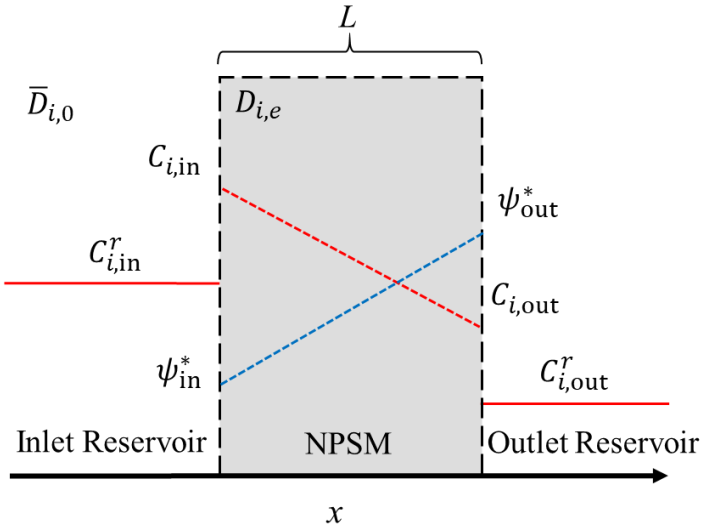

Fig. S2. A schematic of the simplified system in our investigation with the concentration and electrical potential profiles. The corresponding physics notations are also listed.

Temperature-dependent charge regulation model. The silica can be charged on the surface as it is in contact with an aqueous electrolyte caused by the protonation-deprotonation reactions. The protonation of the silanol group is expected in an extremely acidic electrolyte [24], this reaction is not taken into account due to the given nearly neutral pH value (5-8) in this work. Further we also disregard the protonation-deprotonation reaction of doubly Si-coordinated Si_2O groups. In the case of a simple dilute NaCl electrolyte, the simple Basic Stern model has been shown by a previous study to be valid for calculating the charge density of the silica surface [24]. Therefore, the typical reaction on the silica surface can be written as:

$$\text{-SiOH} \rightleftharpoons[K_a]{} \text{-SiO}^- + \text{H}^+, \tag{S10}$$

with the surface dissociation constant $K_a = a\left(\text{-SiO}^-\right)a\left(\text{H}^+\right)/a\left(\text{-SiOH}\right)$, where $a(\cdot)$ denotes the chemical activity of the term in the bracket. As reported in [49, 50], the relationship of surface charge density σ and the surface electrical potential ψ_s follows the basic Stern (BS) model as:

$$\psi_s = \frac{k_b T}{e}\ln\left(\frac{-\sigma}{eN_s+\sigma}\right) + \frac{k_b T}{e}\left[\ln K_{a,T} - \text{pH}\ln(10)\right] - \frac{\sigma}{CS}, \tag{S11}$$

where k_b, e, N_s and CS are the Boltzmann constant, the electron charge, the total surface site density and the capacity of Stern layer, respectively. Herein, $K_{a,T}$ is sensitive to the temperature and determined by using the following van't Hoff equation [10, 20, 51]:

$$\ln\left(\frac{K_{a,T}}{K_{a,Tr}}\right) = -\frac{\Delta H^0_{m,r}}{R}\left(\frac{1}{T}-\frac{1}{T_r}\right), \tag{S12}$$

where $\Delta H^0_{m,r}$ denotes the standard molar reaction enthalpy, $K_{a,Tr}$ the surface dissociation constant at the reference temperature T_r and R the ideal gas constant. Recall that surfac e charge density also satisfies the classical Couy-Chapman formula for a symmetric monovalent electrolyte as [49, 50]:

$$\sigma = \sqrt{8\varepsilon k_b C_0^r RT}\sinh\frac{F\psi_s}{2RT}, \tag{S13}$$

with the permittivity of electrolyte ε, the Faraday constant F and the Boltzmann constant k_b. By using the Newton method, one can numerically solve (S11)-(S13) together to calculate σ with respect to different temperatures and pH. Previous literature indicated that the average surface charge density is less than the value given by the BS model caused by the roughness of the silica surface [35, 36] and the nonlinearity of the Poisson-Boltzmann equation [52]. Therefore, we employ an effective surface charge density $\bar{\sigma} = \alpha\sigma$ connecting to σ by using the scale factor α with a typical range from 0.1 to 0.9. Although ε is a temperature-dependency parameter, its relative rate of variation with respect to the temperature change is $d_T\varepsilon/\varepsilon \approx -5\times10^{-3}\ \text{K}^{-1}$, which is non-significant to affect the value of σ, hence we fix

$\varepsilon = 6.95\times10^{-10}$ C/V·m . The parameters in the BS model are $F = 9.64\times10^{4}$ C/mol , R=8.31 J/(mol×K) , $k_b = 1.38\times10^{-23}$ J/K , $e = 1.60\times10^{-19}$ C , $CS \approx 2.9$ F/m^2 and $N_s \approx 8.0\times10^{18}$ m^{-2} [24]. In this work, the principal temperature-dependency parameter $K_{a,Tr}$ equals to $10^{7.9}$ at $T_r = 298.15$ K , and $\Delta H^0_{m,r} \approx 40\times10^3$ J/mol , which are in the typical range of these parameters [10, 20, 51]. Figure 2-C shows the predictions as a function of pH and temperature by using the proposed model. Generally, $\bar{\sigma}$ decreases versus the reduction of pH value. The relative change rate of $\bar{\sigma}$ with temperature is $d_T\sigma/\sigma \sim \mathrm{O}(10^{-2})$ K^{-1}.

Numerical framework for solving fully coupled Poisson-Nernst-Planck equations.

Herein, to capture the structure of fully overlapping EDL, we directly solve the more fundamental coupled Poisson-Nernst-Planck equations in a two-dimensional nanochannel as:

$$\frac{\partial C_i^p}{\partial t} = \nabla\cdot\left(D_{i,0}\nabla C_i^p + D_{i,0}z_iFC_i^p\nabla\psi_i^p/RT + D_{i,0}S_TC_i^p\nabla T_i\right), \tag{S14}$$

$$\nabla^2\psi_i^p = -\sum_i \frac{Fz_iC_i^p}{\varepsilon}, \tag{S15}$$

where the superscript "*p*" means the corresponding term at the pore scale. An approximate dependence of the diffusion coefficient on the temperature in liquids is generally predicted by the Stokes-Einstein equation [53]:

$$\frac{D_{i,0}(T_1)}{D_{i,0}(T_2)} = \frac{T_1}{T_2}\frac{\mu(T_2)}{\mu(T_1)}, \tag{S16}$$

with the dynamic viscosity $\mu(T_1)$ and $\mu(T_2)$ of electrolyte for corresponding absolute temperature T_1 and T_2. For the ion transport, the zero normal flux boundary condition is applied at the liquid-solid interface while the inlet/outlet uses the constant concentration boundary condition. The electrical boundary condition is applied through surface charge density calculated by the temperature-dependent charge regulation model. Benefiting the high efficiency of the lattice Boltzmann method (LBM) for parallel computing, the LBM is used as our numerical framework in this study. The corresponding numerical lattice evolution equations for concentration and electrical potential have been described in our previous studies [30, 54, 55].

The Poisson equation is solved iteratively in the LBM scheme until the electrical potential convergence is reached at each time step of the evolution of ions. In this investigation, the set of coupled ion and temperature evolution equations in charged clay are solved by the GPU-LBM codes on Tesla-K80 GPU.

REFERENCES

[1] S. Duhr, D. Braun, Why molecules move along a temperature gradient, Proc. Natl. Acad. Sci. U. S. A. 103(52) (2006) 19678-19682.

[2] E.C. Thornton, W.E. Seyfried, Thermodiffusional transport in Pelagic Clay: implications for nuclear waste disposal in geological media, Science 220(4602) (1983) 1156.

[3] K. Chen, L. Yao, B. Su, Bionic thermoelectric response with nanochannels, J. Am. Chem. Soc. 141(21) (2019) 8608-8615.

[4] T. Li, X. Zhang, S.D. Lacey, R. Mi, X. Zhao, F. Jiang, J. Song, Z. Liu, G. Chen, J. Dai, Y. Yao, S. Das, R. Yang, R.M. Briber, L. Hu, Cellulose ionic conductors with high differential thermal voltage for low-grade heat harvesting, Nature materials 18(6) (2019) 608-613.

[5] S. Di Lecce, T. Albrecht, F. Bresme, The role of ion–water interactions in determining the Soret coefficient of LiCl aqueous solutions, Phys. Chem. Chem. Phys. 19(14) (2017) 9575-9583.

[6] J.K. Platten, The Soret effect: a review of recent experimental results, Journal of Applied Mechanics 73(1) (2005) 5-15.

[7] D. Stein, M. Kruithof, C. Dekker, Surface-charge-governed ion transport in nanofluidic channels, Physical Review Letters 93(3) (2004) 035901.

[8] M.A. Glaus, M. Birgersson, O. Karnland, L.R. Van Loon, Seeming steady-state uphill diffusion of 22Na+ in compacted montmorillonite, Environ. Sci. Technol. 47(20) (2013) 11522-7.

[9] A. Wuerger, Thermal non-equilibrium transport in colloids, Reports on Progress in Physics 73(12) (2010) 126601.

[10] M.S. Azam, C. Cai, J.M. Gibbs, E. Tyrode, D.K. Hore, Silica surface charge enhancement at elevated temperatures revealed by interfacial water signals, J. Am. Chem. Soc. 142(2) (2020) 669-673.

[11] A. Alizadeh, M. Wang, Temperature effects on electrical double layer at solid-aqueous solution interface, Electrophoresis 41(12) (2020) 1067-1072.

[12] R. Sprocati, A. Gallo, R. Sethi, M. Rolle, Electrokinetic delivery of reactants: pore water chemistry controls transport, mixing, and degradation, Environ. Sci. Technol. 55(1) (2021) 719-729.

[13] K. Rodríguez, M. Araujo, Temperature and pressure effects on zeta potential values of reservoir minerals, J. Colloid Interface Sci. 300(2) (2006) 788-794.

[14] A. Revil, C. Meyer, Q. Niu, A laboratory investigation of the thermoelectric effect, Geophysics 81(4) (2016) E243-E257.

[15] M. Dietzel, S. Hardt, Thermoelectricity in confined liquid electrolytes, Phys. Rev. Lett. 116(22) (2016) 225901.

[16] Ryzhkov, II, D.V. Lebedev, V.S. Solodovnichenko, A.V. Shiverskiy, M.M. Simunin, Induced-charge enhancement of the diffusion potential in membranes with polarizable nanopores, Phys. Rev. Lett. 119(22) (2017) 226001.

[17] K.D. Sandbakk, A. Bentien, S. Kjelstrup, Thermoelectric effects in ion conducting membranes and perspectives for thermoelectric energy conversion, J. Membr. Sci. 434 (2013) 10-17.
[18] M. Taghipoor, A. Bertsch, P. Renaud, Temperature sensitivity of nanochannel electrical conductance, ACS Nano 9(4) (2015) 4563-4571.
[19] A. Kitamura, K. Fujiwara, T. Yamamoto, S. Nishikawa, H. Moriyama, Analysis of adsorption behavior of cations onto quartz surface by electrical double-layer model, J. Nucl. Sci. Technol. 36(12) (1999) 1167-1175.
[20] A. Revil, P.A. Pezard, P.W.J. Glover, Streaming potential in porous media: 1. Theory of the zeta potential, Journal of Geophysical Research: Solid Earth 104(B9) (1999) 20021-20031.
[21] L.R. Van Loon, J.M. Soler, M.H. Bradbury, Diffusion of HTO, 36Cl− and 125I− in Opalinus Clay samples from Mont Terri, J. Contam. Hydrol. 61(1-4) (2003) 73-83.
[22] M.A. Glaus, M. Aertsens, C.A.J. Appelo, T. Kupcik, N. Maes, L. Van Laer, L.R. Van Loon, Cation diffusion in the electrical double layer enhances the mass transfer rates for Sr2+, Co2+ and Zn2+ in compacted illite, Geochim. Cosmochim. Acta 165 (2015) 376-388.
[23] T.K. Tokunaga, S. Finsterle, Y. Kim, J. Wan, A. Lanzirotti, M. Newville, Ion diffusion within water films in unsaturated porous media, Environ. Sci. Technol. 51(8) (2017) 4338-4346.
[24] M. Wang, A. Revil, Electrochemical charge of silica surfaces at high ionic strength in narrow channels, J. Colloid Interface Sci. 343(1) (2010) 381-386.
[25] T. Colla, M. Girotto, A.P. Dos Santos, Y. Levin, Charge neutrality breakdown in confined aqueous electrolytes: Theory and simulation, J. Chem. Phys. 145(9) (2016) 094704.
[26] J. Colombani, J. Bert, J. Dupuy-Philon, Thermal diffusion in (LiCl, RH 2 O), The Journal of chemical physics 110(17) (1999) 8622-8627.
[27] F. Romer, Z. Wang, S. Wiegand, F. Bresme, Alkali halide solutions under thermal gradients: soret coefficients and heat transfer mechanisms, J. Phys. Chem. B 117(27) (2013) 8209-22.
[28] U. Hornung, Homogenization and porous media, Springer, Springer, 1997.
[29] R. Long, Z. Kuang, Z. Liu, W. Liu, Temperature regulated reverse electrodialysis in charged nanopores, J. Membr. Sci. 561 (2018) 1-9.
[30] Y. Yang, M. Wang, Pore-scale study of thermal effects on ion diffusion in clay with inhomogeneous surface charge, J. Colloid Interface Sci. 514 (2018) 443-451.
[31] R.F. Probstein, Physicochemical hydrodynamics: an introduction, John Wiley & Sons2005.
[32] H. Ohshima, S. Ohki, Donnan potential and surface potential of a charged membrane, Biophys. J. 47(5) (1985) 673-678.
[33] A.D. MacGillivray, Nernst - Planck equations and the electroneutrality and Donnan equilibrium assumptions, The Journal of Chemical Physics 48(7) (1968) 2903-2907.

[34] J.S. Duncan, Introduction to colloid and surface chemistry, Elsevier Science Ltd, 1992.
[35] B.O. Alan, M. Barisik, H.G. Ozcelik, Roughness effects on the surface charge properties of silica nanoparticles, The Journal of Physical Chemistry C 124(13) (2020) 7274-7286.
[36] H.G. Ozcelik, M. Barisik, Electric charge of nanopatterned silica surfaces, Phys. Chem. Chem. Phys. 21(14) (2019) 7576-7587.
[37] B. Ghanbarian, A.G. Hunt, R.P. Ewing, M. Sahimi, Tortuosity in porous media: a critical review, Soil Sci. Soc. Am. J. 77(5) (2013) 1461-1477.
[38] A.W. Miller, Y. Wang, Radionuclide interaction with clays in dilute and heavily compacted systems: a critical review, Environ. Sci. Technol. 46(4) (2012) 1981-1994.
[39] H. Tian, L. Zhang, M. Wang, Applicability of Donnan equilibrium theory at nanochannel-reservoir interfaces, J. Colloid Interface Sci. 452 (2015) 78-88.
[40] R.P. Misra, J.P. de Souza, D. Blankschtein, M.Z. Bazant, Theory of surface forces in multivalent electrolytes, Langmuir 35(35) (2019) 11550-11565.
[41] Y. Yang, M. Wang, Cation diffusion in compacted clay: a pore-scale view, Environ. Sci. Technol. 53(4) (2019) 1976-1984.
[42] M. Maldovan, Sound and heat revolutions in phononics, Nature 503(7475) (2013) 209-17.
[43] R. Schittny, M. Kadic, S. Guenneau, M. Wegener, Experiments on transformation thermodynamics: molding the flow of heat, Phys. Rev. Lett. 110(19) (2013) 195901.
[44] S. Narayana, Y. Sato, Heat flux manipulation with engineered thermal materials, Phys. Rev. Lett. 108(21) (2012) 214303.
[45] C.W. Chang, D. Okawa, A. Majumdar, A. Zettl, Solid-state thermal rectifier, Science 314(5802) (2006) 1121.
[46] Y. Ye, G. Chiogna, O.A. Cirpka, P. Grathwohl, M. Rolle, Experimental evidence of helical flow in porous media, Phys. Rev. Lett. 115(19) (2015) 194502.
[47] Q. Sun, D. Wang, Y. Li, J. Zhang, S. Ye, J. Cui, L. Chen, Z. Wang, H.J. Butt, D. Vollmer, X. Deng, Surface charge printing for programmed droplet transport, Nature materials 18(9) (2019) 936-941.
[48] C. Malmberg, A. Maryott, Dielectric constant of water from 0°C to 100°C, Journal of research of the National Bureau of Standards 56(1) (1956) 1-8.
[49] J. Lyklema, Fundamentals of interface and colloid science. Volume 2: Solid-liquid interfaces. , Fundamentals of interface and colloid science. Volume 2: Solid-liquid interfaces. , Kolloidnyi Zhurnal1995.
[50] R.J. Hunter, Foundations of colloid science, Oxford University Press2001.
[51] P.M. Reppert, Temperature-dependent streaming potentials: 1. Theory, Journal of Geophysical Research 108(B11) (2003).
[52] S.H. Behrens, D.G. Grier, The charge of glass and silica surfaces, The Journal of Chemical Physics 115(14) (2001) 6716-6721.
[53] R. Kubo, The fluctuation-dissipation theorem, Rep. Prog. Phys. 29(1) (1966) 255.

[54] M. Wang, N. Pan, Predictions of effective physical properties of complex multiphase materials, Materials Science and Engineering: R: Reports 63(1) (2008) 1-30.
[55] L. Zhang, M. Wang, Modeling of electrokinetic reactive transport in micropore using a coupled lattice Boltzmann method, Journal of Geophysical Research: Solid Earth 120(5) (2015) 2877-2890.